Project Final Progress Report

Funding Agency/ Program: Interstate Shellfish Sanitation Conference/ Techniques and Practices for *Vibrio* Reduction and Techniques and Tools for Toxin Management

Project Title: Influence of Plankton Community Composition and Abiotic Environmental Factors on the Dynamics of Total and Pathogenic *Vibrio parahaemolyticus* in Oysters, Water and Sediment

Organization: Virginia Institute of Marine Science, College of William & Mary

Project Location: Gloucester Point, Virginia

Requested Project Period: September 1, 2018–April 1, 2020

Principal Investigator: Dr. Corinne Audemard–Associate Research Scientist

Co-Principal Investigators: Dr. Kimberly S. Reece–Professor
Dr. Deborah K. Steinberg–Professor
Dr. William G. Reay–Research Associate Professor

Influence of Plankton Community Composition and Abiotic Environmental Factors on the Dynamics of Total and Pathogenic *Vibrio parahaemolyticus* in Oysters, Water and Sediment

1. Objectives

In this study, we evaluated the influence of abiotic environmental factors and biotic factors including phytoplankton and zooplankton species composition on relative abundance on the occurrence of total pathogenic *Vibrio parahaemolyticus* (*Vp*) in oysters, water and sediment while also assessing potential correlations between pathogenic and total *Vp*.

The specific objectives of the project were to:

- Evaluate the influence of a wide array of abiotic and biotic environmental factors on levels of total and pathogenic *Vp* in 3 matrices: oysters, water and sediment;
- Evaluate potential correlations between levels of total and pathogenic *Vp* for each matrice as well as potential correlations between levels of *Vp* measured in the different matrices;
- Provide science-based data to the ISSC, to other regulatory agencies and researchers to foster improved *Vp* risk management measures and predictive models.

2. Methods

a. Study sites

The study was conducted in the York River, an estuary located in lower Chesapeake Bay. One site was adjacent to the Virginia Institute of Marine Science (VIMS), Virginia (37°14′52.0″ N, 76°29′59.5″ W), and the second was located in Perrin Creek, a tributary of the York River in proximity to the VIMS site (Fig. 1). These sites were chosen based on similar moderate salinity regime and differences related to exposure to flushing and hydrodynamics that may affect environmental conditions and, potentially, affect *Vp* dynamics.

A month prior to sample collection started, triploid oysters of commercial size (> 50 mm) were deployed in 3 bags each containing 140 oysters placed on racks at both study sites. Oyster, water and sediment samples were collected from both sites on the same day approximately every two weeks from April 30, 2019 to August 5, 2019 leading to a total of 8 sampling time points. Samples were collected within 1 hour of low tide across all sampling time points. In addition, near-continuous (15 mins interval) water quality measurements using YSI® multi-parameter water quality sondes were collected (Table 1).

b. Environmental Factors

Near continuous (15-minutes interval) *in situ* measurements of selected water quality parameters (Table 1) was collected immediately adjacent to each of the grow-out sites at a fixed depth (approximating that of exposed oysters) using YSI® multi-parameter water quality sondes.

Measured parameters included temperature (resolution: 0.01 °C, accuracy: ± 0.15 °C), specific conductance (0.001 mS/cm, ±0.5% of reading), pH (0.01 SU, ± 0.2 SU), $\%DO_{sat}$ (0.1%, ±1% of reading), turbidity (1 NTU, ± 0.2% of reading) and Chl-a fluorescence (~0.1 µg/L, 0.1% of RFU). Calculated parameters included salinity (0.01 psu, ±1% of reading) and [DO] (0.01 mg/L, 1% of reading). Water depth (0.001 m; ± 0.01 m) was also be measured via the sonde with the non-vented pressure sensor being corrected for atmospheric pressure changes during the deployment period. Configuration and calibration of YSI® instruments followed standard protocols. All efforts, including short maintenance intervals (~1 week), use of self-cleaning optical sensors, and anti-fouling material; was taken to minimize biofouling effects. Data were subjected to quality assurance/quality control (QA/QC) protocols and archived through the VA Estuarine and Coastal Observing System portal (www.web2.vims.edu/vecos). QA/QC protocols tested for time gaps and location errors, syntax errors, gross sensor output range, temporal range, positive and negative spikes, rate of change, continuously reported values, and sensor drift.

Dissolved nutrients and plant pigments (Table 1) were measured using standards methods for marine waters, these include: ammonium (NH_4; Solorzano 1969), nitrate + nitrite (NO_{23}; Strickland and Parsons 1968, total dissolved nitrogen (TDN; D'Elia et al. 1977), reactive and total phosphorus (PO_4 and TDP; Method 365.5 direct and digestion colorimetry, EPA 1997), total chlorophyll a and pheopigments (Arar & Collins 1997. Method 445.0.). Field samples were collected at each sampling time point and were placed on ice and immediately filtered and analyzed.

In addition, a sediment sample was collected at the beginning of the study for assessing general characteristics and differences between the 2 study sites. Surficial (top 1 cm) sediment samples were collected manually with transparent plexiglass cores (I.D.: 4.6 cm) and were categorized into gravel, sand (coarse, medium, fine), silt and clay using the Wentworth scale following a wet-sieve and pipette analysis (Folk 1980).

c. *Phytoplankton species composition and abundance*

Triplicate 100 mL water samples were collected from each site to assess relative abundance of phytoplankton species at each sampling time point. One water sample was analyzed for microscopic examination and visual enumeration of dominant phytoplankton species. A second water sample was preserved with Lugol's iodine for additional confirmatory microscopic examination and the third water sample was filtered through a 3 µm Isopore™ membrane filter (Millipore Corp) for molecular method analysis. DNA was extracted from these filters using the QIAamp ® Fast Stool Mini Kit (QIAGEN) following the manufacturer's protocol. Species-specific qPCRs were conducted to determine cell densities of typical HAB summer bloom species in the York River. Specifically, a different qPCR assay was run for each of the 4 dinoflagellate species: *Alexandrium monilatum* (Vandersea et al. 2017), *Margalefidinium polykrikoides* (Reece et al. in VA-DEQ 2014), *Karlodinium veneficum* (Reece et al. in VA-DEQ 2014) and *Prorocentrum minimum* (Handy et al. 2008). Clonal cultures of each species are maintained in the Reece laboratory so that DNA can be extracted from a known number of cells to use as positive control material and for generating standard curves. qPCR assays were done on a 7500 Fast Real-Time PCR system (Life Technologies) using the Fast 7500 mode with the cycling parameters, reagent concentrations as previously described (Reece et al. in VA-DEQ 2014, Vandersea et al. 2017).

d. *Zooplankton species composition and abundance*

Relative abundance of zooplankton species was assessed at each sampling time point using a 200 µm, 0.5 m diameter ring net with attached flowmeter. Zooplankton tow samples were collected from a pier located at VIMS and from a dock located at Perrin Creek site. Zooplankton was enumerated and identified to the lowest taxonomical level possible using an Olympus SZH12 bright/darkfield dissecting microscope. Relative abundance of each taxon was assessed using densities of each taxon (abundance divided by the volume of water through the net, i.e., number per liter) (Condon & Steinberg 2008).

e. *Vibrio* spp. abundance in oyster, sediment and water samples

At each sampling time point and at each site, triplicate samples of 10 oysters each, triplicate surface sediment samples and triplicate 100 ml water sample were collected. Samples were kept chilled in insulated coolers and separated from direct contact with ice during transport. Upon arrival at the laboratory, samples were processed using a most-probable number (MPN) approach followed by quantitative PCR (qPCR) to determine the abundance of total and pathogenic *Vp*.

For each oyster replicate sample, a tissue homogenate was prepared by pooling tissue and liquor of 10 oysters, adding an equal weight of phosphate-buffered saline (PBS) and homogenizing for 90 s (US FDA 2010). Sediment samples were diluted 1:1 in PBS and vortexed to release bacteria attached to particles (Chase et al. 2015). For each of these tissue homogenate or vortexed sediment sample, tenfold serial dilutions were prepared using PBS before being inoculated into 10 ml of alkaline peptone water (APW) following a 3 tube MPN series (US FDA 2010). The obtained g equivalent inoculated for these oyster and sediment samples ranged from 1.00E+0 g to 1.00E-5 g.

For the water samples, in addition to serial dilution of the water inoculated into APW (1.00E+0 ml to 1.00E-4 ml inoculate), the equivalent of a 10 ml inoculate was prepared. The objective was to enhance our ability to detect low *Vp* abundance, in particular low pathogenic *Vp* abundance in the samples. Each of triplicate 10 ml samples were filtered on a 0.22 µM filter, which was then placed in a sterile tube containing 1 ml of PBS. Bacteria were released from the filter by vortexing the content of the tubes and the entire content of the tube including the fitter was added to APW. All inoculated samples were incubated at 35°C for 18-24 h.

A 100 µl volume was removed from the top cm of each APW enrichment tube showing turbidity and was boiled for 10 min to lyse cells (Jones et al. 2009). This lysate was subsequently used as the source of template DNA in each of the qPCR assays described below.

Detection of total and pathogenic *Vp* was performed using the primers and probes described by Nordstrom et al. (2007) with the modifications recommended by the FDA Gulf Coast Seafood Laboratory (J. Jones pers. comm.). Total *Vp* was detected by targeting the thermolabile hemolysin gene (*tlh*) in a multiplex qPCR assay incorporating an internal amplification control (IAC) to ensure PCR integrity and eliminate false-negative reporting. Detection of *Vp* pathogenic strains possessing the *tdh* and/or the *trh* gene was conducted in a second qPCR assay that also includes an IAC. In cases where the IAC did not amplify correctly compared to the controls, the qPCR for the corresponding sample(s) was repeated. Results of the qPCRs were used to assess the MPN density values using approved MPN tables (US FDA 2010).

f. Data analysis

For each matrix, percentage of occurrence of each targeted gene (*tlh*, *tdh* and *trh*) was calculated after grouping the data obtained from each of the 2 sites, i.e., by using the data obtained from 6 samples (3 replicates from Perrin and 3 replicates from York). For *Vibrio* abundance data, the geometric means of triplicate samples obtained for each matrix and at each time point were calculated and presented graphically. In cases where the targeted gene was not detected (below detection limit), the specific sample was given a value for that gene corresponding to the lower limit of detection (0.3 MPN/g or 0.03 MPN/ml).

Spearman's rank correlation coefficients were calculated to assess 1/ the correlations between levels of either *tlh*, *tdh or trh* between matrices and, 2/ the correlations between levels of *tlh* and levels of *tdh* or of *trh* within each matrix (oyster, sediment and water).

For each targeted *Vp* strains (*tlh*, *tdh* or *trh*), identification of environmental predictor variable affecting the abundance of these strains in the different matrices was conducted using generalized additive mixed-effects models (GAMMs), which extend generalized additive models (GAM) by including both fixed and random effects. These models can be useful for situations where the nonlinear functions of predictor variables are needed, and for hierarchical data with autocorrelation due to repeated temporal sampling. GAMMs are expressed as:

$$g\big(E(\mathbf{y}|\mathbf{b})\big) = \mathbf{X}\boldsymbol{\beta} + \sum_{j=1}^{p} s_j(x_j) + \mathbf{Z}\mathbf{b}$$
$$\mathbf{b} \sim \mathrm{N}(\mathbf{0}, \boldsymbol{\Sigma})$$

where $E(\mathbf{y}|\mathbf{b})$ is the expected value of the response vector $\mathbf{y}$ conditioned on the vector of random effects $\mathbf{b}$ that are independent and identically normally distributed, $\mathbf{X}\boldsymbol{\beta}$ is the fixed-effect linear parametric model component, $s_j(x_j)$ are the nonparametric, smooth, and nonlinear functions of predictor variables ($j = 1, \ldots, p$), $\mathbf{Z}\mathbf{b}$ is the random-effect model component, $\boldsymbol{\Sigma}$ is the variance-covariance matrix of the random effects, and g is the monotonic link function.

The fixed-effect predictors considered were the aforementioned abiotic and biotic factors measured synoptically with *Vp*. Sampling time was treated as a random-effect and assumed to only influence the intercept (random intercept model). In this formulation, $\mathbf{Z}$ is a simple dummy matrix denoting sampling time and $\boldsymbol{\Sigma}$ is a diagonal matrix with the sampling time variance σ^2_{time} along the diagonal.

Statistical models were fitted the generalized additive models for location, scale, and shape (GAMLSS) regression framework (Stasinopoulos et al. 2017) implemented through the *gamlss* package in R (R Core Team, 2018). GAMLSS models extend generalized linear and additive mixed effects models in two important ways: (i) a wider range of distributions for the response variable are allowed compared to those included in the exponential family, including distributions that are heavy or light-tailed, positively or negatively skewed, and (ii) all parameters of the distributions, namely location (mean or median), scale (variance), and shape (skewness and kurtosis) can be modeled as linear or smooth functions of predictor variables.

For each strain of *Vp* from each medium, a variety of model parameterizations was fitted to develop the most parsimonious description of the data. The zooplankton abundance data were converted into a proportion to the total number of zooplankters observed. Model selection and statistical inference will be guided by Akaike's Information Criterion (AIC), the Bayesian Information Criterion (BIC), and standard model diagnostics such as QQ plots, detrended quantile-quantile plots also known as worm plots, and analyses of residuals. Marginal mean predictions (Searle et al. 1980) was generated from the selected model and uncertainty in the

form of standard errors and/or confidence intervals of predictions was quantified from 1000 nonparametric bootstrapped samples (Efron and Tibshirani 1993).
Analysis were conducted under R (R core Team, 2017).

3. **Results**

a. Environmental factors

General sediment characteristics reflected the hydrodynamic setting of the sites. Perrin located in a small shallow creek with low flow, was characterized by about equal proportion of sand, silt and clay, while York located in a large estuary, was characterized by sediment almost exclusively composed of sand (Table 2). These 2 sites also showed slightly different range of water temperature and salinity (Table 3; Fig. 2). Perrin was associated with slightly warmer water temperature (20.91 to 30.81˚C) compared to York (18.15 to 27.91˚C) and with slightly lower salinity (13.08 to 17.91 psu) than at York (13.85 to 19.37 psu). Perrin was also associated with lower mean turbidity (6.88 ± 4.23 NTU) than York (10.13 ± 4.58 NTU) with higher turbidity values observed at this later site mid-June and mid-July. Based on the trends observed using YSI sensors data, Perrin was associated with chlorophyll a increases in May and late July, while York was associated with chlorophyll a increases in April and mid-July. In grab samples collected at time of sampling, chlorophyll a measured during the course of the study covered a wider range of values at Perrin (8.94 to 35.96 µg/L) compared to York (9.10 to 25.39 µg/L). Average pH and DO values recorded at time of sampling suggested lower pH and DO at Perrin compared to York, however, DO measured at York varied more widely than at Perrin with a pronounced decrease observed late July after a rain event (data not shown).

Additional water quality data acquired through grab samples are shown in Fig. 3. As noted above, the 2 studied sites show different chlorophyll a dynamic but they also were associated with different total suspended solid dynamics with the highest values observed at Perrin on May 28 (40.50 mg/L), and at York on August 5 (39.33 mg/L). Finally, both dissolved organic nitrogen and total dissolved phosphorus showed higher values at Perrin than at York.

b. Phytoplankton species composition and relative abundance

Taxa identified by visual counts during this study included 2 diatom species (*Bacillaria* sp. and *Pseudo-nitzchia* sp.), diatoms, filamentous diatoms, 3 dinoflagellates species (*Akashiwo sanguinea*, *Heterocapsa rotundata* and *Pheopolykrikoides hatmanii*) and a group consisting of unidentified chlorophytes and dinoflagellates. This later group as well as the diatoms and filamentous diatoms were associated with the highest counts measured in either site (Fig. 4). The highest abundance measured for the group of unidentified chlorophytes and dinoflagellates (395 cells/mL) was recorded at Perrin on April 30. The highest count for diatoms (295 cells/mL) and filamentous diatoms (195 cells/mL) were recorded at York on both June 10 and June 27. None of these taxa reached abundance susceptible to form blooms.

Among the 4 dinoflagellate species analyzed by qPCR, *A. monilatum* and *M. polykrikoides* were seldomly detected and showed very low concentration < 0.5 cell/mL so the associated data were not plotted on Fig. 4. *P. minimum* was detected more often during the course of the study (Fig. 4), but abundance was low with the highest value recorded at York on

April 30 (267 cells/mL). *K. veneficum* showed a similar dynamic at both study sites with the highest concentrations observed in May and April (up to 428 cells/mL at Perrin on May 14).

c. Zooplankton species composition and relative abundance

Among the zooplankton taxa identified, Balanidae nauplius and cypris, the copepod species *Acartia* (*Acanthartia*) *tonsa*, Cladocera, invertebrate eggs, *Uca* sp. larvae (fiddler crab larva), polychaeta larva and Gastropoda larva dominated in terms of relative abundance (Fig. 5). At Perrin, Balanidea dominated during the first three sampling time point (late April to late May). At this site, the following sampling time point were associated with other dominant taxa, such as Invertebrata eggs on June 10, *A. tonsa* in June and in July and *Uca* larva on August 5. While Balanidae also dominated on April 30 at York, the relative abundance of this group was not as elevated as at Perrin in May. At the York site, Cladocera was the dominant taxon on May 14 but from May 28 till August 5, *A. tonsa* was the dominant taxon.

The range of abundance observed varied with the site, with an overall higher abundance of zooplankter observed at York compared to Perrin (Fig. 6). More specifically, the groups that were associated with higher abundance values at York compared to Perrin were the Copepoda, Cladocera, Balanidae larva, and Mollusca larva.

d. Prevalence of total and pathogenic *Vp* in sediment, oyster and water

Detection of the *tlh* gene associated with all *Vp* strains, was observed for all replicate samples across all sample matrices with the exception of one oyster replicate sample collected at the York site on April 30. At both sites, *tdh* and *trh* genes associated with potentially virulent strains, were detected at each sampling time point in at least one type of matrix. Data for each site were pooled to illustrate rate of detection of these genes in each matrix at each time point (Fig. 7).

Detection of *tdh* occurred in all oyster samples collected in May and June. During the rest of the study, rate of detection of this gene in oyster samples range from 16% (April 30) to 83% (July and early August). In this matrix, the *trh* gene was detected in all the samples collected in May and on June 10. Lower rates of detection were observed on April 30 (16%) and from July through early August (33-66%).

In sediment samples, detection of the *tdh* gene was observed on all but one sample collected at the York site on April 30. Similarly, sediment samples were associated with a high rate of detection of the *trh* gene with all samples collected from April 30 to July 10 being positive for this gene.

In water samples, *tdh* gene was detected in all samples collected on May 28, June 10, July 10 and July 23. The rest of the sampling time points were associated with rates of the detection ranging from 33% (August 5) to 66% (June 27). Detection of the *trh* gene in water samples was 100% on May 14 and on June 10 and ranged from 33 to 83% at the other time points.

e. Abundance of total of pathogenic *Vp* in sediment, oyster and water

As shown on Fig. 8 depicting *tlh* geometric means at each site and in each matrix, total *Vp* abundance were the lowest on April 30. Comparing equivalent unit of weight and volume

(i.e. MPN/g and MPN/ml), the overall range of values observed varied with the matrix with the following trend: sediment > oyster > water. Mean abundance of *tlh* in sediment ranged from 3.32E+2 MPN/g to 8.87E+4 MPN/g at Perrin and from 7.08E+2 to 4.85E+4 MPN/g at the York site. In oyster samples, mean abundance of *tlh* ranged from 7.19E+1 to 8.91E+3 MPN/g at Perrin and from 2.00E+0 to 4.19E+4 MPN/g at York. Finally, mean abundance of *tlh* in water samples ranged from 2.13E+1 to 1.58E+3 MPN/ml at Perrin and from 4.57E-1 to 9.22E+2 MPN/ml at York.

Higher abundance of *tdh* and *trh* genes were observed in sediment samples compared to oyster and water samples (Fig. 9). Mean *tdh* abundance in sediment samples ranged from 7.10E+0 to 4.60E+2 MPN/g at Perrin and from 4.77E-1 to 9.46E+1 MPN/g at York. Mean *trh* abundance ranged from 5.63E-1 to 7.24E+0 MPN/g at Perrin and from 3.18E-1 to 4.70E+1 MPN/g at York. Mean *tdh* abundance in oyster samples ranged from 3.50E-1 to 7.81E+1 MPN/g at Perrin and from 3.5E-1 to 7.99E+0 MPN/g at York. In the same matrix, mean *trh* abundance ranged from 3.17E-1 to 2.77E+0 MPN/g at Perrin and from 3.17E-1 to 2.24E+0 MPN/g at York. Finally, in water samples, mean *tdh* abundance ranged from 7.00E-2 to 3.20E-1 MPN/ml at Perrin and from 3.50E-2 to 3.80E-1 MPN/ml at York. Mean *trh* abundance in these samples ranged from 3.00E-2 to 3.20E-1 MPN/ml at Perrin and from 3.33E-2 to 2.00E-1 MPN/ml at York.

f. Correlation between strains and between matrices

Abundance of total *Vp* in water and in oyster were found to be correlated ($r = 0.520$, $p < 0.05$) but abundance of these strains in the sediment was not correlated to the abundance in other matrices (Table 4). Levels of *tdh* measured within each matrix analyzed were correlated with each other. For *trh* strains, levels measured in water were correlated to levels measured in sediment and in oyster.

In oysters, there was no significant association between total and pathogenic *Vp* (*tdh* or *trh*) (Table 5). Within the sediment and the water, levels of *tdh* were found to be significantly correlated to levels of total *Vp*. No significant correlation was observed between levels of total *Vp* and levels of *trh*.

g. Influence of abiotic and biotic environmental parameters

Using GAMMs models and the approach described above, the 2 best models describing *tlh* abundance in oysters included DON with a non-linear relationship or included DON, *K. veneficum* and *Balanidae* larvae (Fig. 10). In sediment samples, the best model for *tlh* included Balanidae larvae with a negative relationship (Fig. 11) and in water samples, the best model for *tlh* included DON and Diatoms, both with a positive relationship but also *P. minimum* with a negative relationship (Fig. 12).

For *tdh* in oysters, the best model included total suspended solid with a negative relationship (Fig. 13). The best models describing *tdh* in sediment included either *P. minimum* or Polychaeta larvae both with a negative relationship (Fig. 14) and the 2 best models for *tdh* in water included either TSS with a non-linear relationship or salinity and *P. minimum,* both with a negative relationship (Fig. 15).

For *trh* in oysters, the best model included only the Cladocera with a positive relationship (Fig. 16). In sediment samples, the model describing *trh* abundance included DON

with a non-linear relationship (Fig. 17) and in water samples the best models included either DON or Cladocera both with a positive relationship (Fig. 18).

4. Discussion and Conclusions

Based on GAMMs models, the identified predictor variables varied with the targeted strains and matrices. Nevertheless, we observed that for each targeted gene (*tlh*, *tdh* or *trh*) some variables were identified as predictor in more than one matrix. This was the case for *tdh*, for which total suspended solid (TSS) was identified as the predictor variable describing the abundance of *tdh* in oysters with a negative relationship but also describing the abundance of *tdh* in the water, although in this case, the relationship was not linear. In the case of *trh*, the only two variables identified as predictor during the analysis of oyster, sediment and water samples were dissolved organic nitrogen (DON) and the crustaceans Cladocera. Finally, for total *Vp*, the recurring variables identified as predictor in the different matrices were DON and Balanidae larvae (barnacle larvae). These observations suggest that total and pathogenic *Vp* strains respond to different environmental factors, but they also suggest that these **specific abiotic or biotic factors may influence the abundance of these strains in more than one matrix.**

In some instances, the obtained models were associated with uncertainties that can be explained by the overall small number of data points relative to the high number of predictor variables included in the analyses. The analyses presented here were run with limited *a priori* grouping of variables in particular for the phytoplankton and zooplankton. High uncertainties were for example observed when the identified predictor variables were the phytoplankton species *K. veneficum* and *P. minimum*, or the zooplankton group such as Balanidae larvae, Cladocera, or Polychaeta larvae. In these cases, the relationship with *Vp* was strongly influenced by a few high values of the predictor variables. Future data analyses may benefit from additional grouping of variables to enhance model strength and/or from the collection of additional data to enhance the number of values associated with predictor variables.

Independently of the matrix, levels of *tdh* strains were overall more elevated at the low energy site (Perrin) compared to the high energy site (York). Such trend was not observed for total *Vp* or for the *trh* positive strains, which showed an opposite trend to *tdh* with a tendency to be associated with higher levels at York compared to Perrin. **These observations suggest that pathogenic *Vp* strains are diverse not only in terms of their genetic profile but also in terms of their response to the environment.** The site general characteristics in terms of hydrodynamics as well as depth, may directly or indirectly influence the dynamics of *Vp* pathogenic strains and may need to be taken into consideration in studies focusing on the ecology of *Vp*.

The differences in levels of pathogenic *Vp* strains also suggest that the approach chosen in this study in terms of study sites known to differ in terms of hydrodynamic while being exposed to overall similar temperature and salinity regime due to their proximity, may foster a better understanding of the factors influencing the abundance of *Vp* pathogenic strains in the environment. Studies focusing on small spatial scale may also help define the spatial distribution of these strains on scales relevant to oyster aquaculture and help inform the areas needed to be tested, and potentially closed for harvest, in cases of outbreaks related to oyster consumption.

Within the studied sites, abundances of total and pathogenic *Vp* were **more elevated in sediment samples compared to oyster and water samples**. Relative higher abundance of *Vp* in sediment compared to other matrices has been observed at other sites (Vezzulli et al. 2009; Johnson et al. 2012) suggesting a key role of the sediment in the ecology of *Vp*. A study conducted in Alabama found relative higher abundance of *Vp* in oysters compared to sediment or water samples (Givens et al. (2014), however, this study was conducted in the winter so the observed different trend may be related to the sampling season (winter in Alabama versus summer in this study) or be related to other factors associated with the study sites.

Compared to previous studies conducted in the York river, overall levels of *tdh* and *trh* detected in oyster and water samples in this study were about 10 to 100 fold lower. Year to year variability likely occurs but the actual environmental condition driving differences between years is not known and merit further investigation, especially in the context of risk prediction. While levels of these pathogenic strains were low, our approach, in particular the inoculation of up to 1 g of oyster homogenate or of sediment, and the inoculation of up to 10 ml of water (after filtration), enhanced our **ability to detect these low abundance strains** and our ability to describe their ecology.

While overall abundance of pathogenic *Vp* appeared low, the observed **higher rate of detection of *tdh* and *trh* strains occurring in May and June** especially in the oyster samples, was similar to what was observed at these sites previously. Low rate of detection of these strains in April can be explained by the relative low water temperature (< 21˚C) occurring at that time but the low rate of detection observed later in the summer seem to be related to other factors such as the one identified using GAMMs models (see above).

In oyster samples, *tdh* and *trh* abundances were not correlated to the abundance of total *Vp*. The absence of correlation between levels of total and pathogenic *Vp* in oysters has been observed elsewhere and it is generally thought that pathogenic *Vp* strains respond to different environmental conditions compared to total *Vp* and/or that levels observed in oysters are influenced by the oyster itself (DePaola et al. 2003; Zimmerman et al. 2007; Johnson et al., 2012; Williams et al. 2017; Flynn et al. 2019). Interestingly, levels of *tdh* in sediment and water were correlated between each other. Although sites differ in their hydrodynamic regime, both sampling sites were shallow (< 2 m), which may explain this observation.

In conclusion, we showed that taking into consideration both biotic and abiotic variables and the choice of study sites of contrasting hydrodynamic conditions, may foster a better understanding of the ecology of total and pathogenic *Vp* in the environment. Although this study was limited in its number of sampling time points, it may provide valuable information relative to the ecology of total and pathogenic *Vp* in the lower Chesapeake and may guide the design of future studies.

5. Bibliographical references

Arar E.J. and Collins. G.B. 1997. Method 445.0. *In Vitro* determination of chlorophyll a and pheophytin a in marine and freshwater algae by fluorescence. Revision 1.2. National Exposure Research Laboratory. Office of Research and Development. U.S. Environmental Protection Agency.

Audemard, C., H.I. Kator, K.M. Reece. 2018. High salinity relay as a post-harvest processing method for reducing *Vibrio vulnificus* levels in oysters (*Crassostrea virginica*). Int. J. Food Microbiol. 279, 70-79.

Baker, G.L. 2016. Food safety impacts from post-harvest processing procedures of molluscan shellfish. Foods 5, 1-12.

Chase, E., Young, S., Harwood, V.J. 2015. Sediment and vegetation as reservoirs of *Vibrio vulnificus* in the Tampa Bay estuary and Gulf of Mexico. Appl. Environ. Microbiol. 81:2489-2494.

Cox AM, Gomez-Chiarri M. 2012. *Vibrio parahaemolyticus* in Rhode Island coastal ponds and the estuarine environment of Narragansett Bay. Appl. Environ. Microbiol. 78:2996–2999.

Davis, B.J.K, Jacobs, J.M., Davis, M.F., Schwab, K.J., DePaola, A., Curriero, F. 2017. Environmental determinants of *Vibrio parahaemolyticus* in the Chesapeake Bay. Appl. Environ. Microbiol. 83:1-15.

Dean, W.E., Jr. 1974. Determination of carbonate and organic matter in calcareous sediments and sedimentary rocks by loss on ignition: Comparison of methods. J. Sediment. Petrol. 44(1): 242-248.

D'Elia, C.F.; Steudler, P.A. and Corwin N. 1977. Determination of total nitrogen in aqueous samples using persulfate digestion. Limnol. Ocean. 22: 760-764.

DePaola, A., Nordstrom, J.L., Bowers, J.C., Wells, J.G., Cook, D.W. 2003. Seasonal abundance of total and pathogenic *Vibrio parahaemolyticus* in Alabama oysters. Appl. Environ. Microbiol. 69, 1521-1526.

Deter, J., Lozach, S., Veron, A., Chollet, J., Derrien, A., Hervio-Heath, D. 2010. Ecology of pathogenic and non-pathogenic *Vibrio parahaemolyticus* on the French Atlantic coast. Effects of temperature, salinity, turbidity and chlorophyll a. Env. Microb. 12:929-937.

EPA 600/R-97/072. 1997. Method 365.5 Determination of orthophosphate in estuarine and coastal waters by automated colorimetric analysis. In: *Methods for the determination of chemical substances in marine and estuarine environmental matrices*. 2nd Edition. National Exposure Research Laboratory, Office of Research and Development. U.S. EPA, Cincinnati, Ohio 45268.

FAO/WHO [Food and Agriculture Organization of the United Nations/World Health Organization]. 2011. Risk assessment of *Vibrio parahaemolyticus* in seafood: Interpretative summary and Technical report. Microbiological Risk Assessment Series No. 16. Rome. 193pp

Flynn A., Davis B.J.K., Atherly E., Olson G. Bowers J.C., DePaola A., Curriero F.C. 2019. Associations of Environmental Conditions and *Vibrio parahaemolyticus* Genetic Markers in Washington State Pacific Oysters. Frontiers Microbiol. 10:2797

Folk, R.L. 1980. *Petrology of Sedimentary Rocks*. Austin, Texas: Hemphill Publishing Company.

Handy, S.M., Demir, E., Hutchins, D.A., Portune, K.J., Whereat, E.B., Hare, C.E., Rose, J.M., Warner, M., Farestad, M., Cary, S.C., Coyne, K.J. 2008. Using quantitative real-time PCR to study competition and community dynamics among Delaware Inland Bays harmful algae in field and laboratory studies. Harmful Algae. 7:599-613.

Johnson, C.N., Bowers, J.C., Griffitt, J., Molina, V., Clostio, R.W., Pei, S., Laws, E., Paranjpye, R.N., Strom, M.S., Chen, A., Hasan, N.A., Huq A., Noriea III, N.F., Grimes, J., Colwell, R.R. 2012. Ecology of *Vibrio parahaemolyticus* and *Vibrio vulnificus* in the coastal and estuarine waters of Louisiana, Maryland, Mississippi, and Washington (United States). Appl. Environ. Microbiol. 78, 7249-7257.

Jones, J.L., Noe, K.E., Byars, R., DePaola, A. 2009. Evaluation of DNA colony hybridization and real-time PCR for detection of *Vibrio parahaemolyticus* and *Vibrio vulnificus* in postharvest-processed oysters. J. Food Prot. 72, 2106–2109.

Kaneko, T. & R.R. Colwell (1975) Adsorption of *Vibrio parahaemolyticus* onto chitin and copepods. Appl. Microbiol. 29(2):269-274.

Martinez-Urtaza, J., Baker-Austin, C., Jones, I.L., Newton, A.E., Gonzalez-Aviles, G.D., DePaola, A. 2013. Spread of the Pacific Northwest *Vibrio parahaemolyticus* strain. N. Engl. J. Med. 369:1573-1574.

Muth, M.K., Viator, C., Karns, S.A., Cajka, J.C., O'Neil, M, 2013. Analysis of the costs and economic feasibility of requiring postharvest processing for raw oysters. Comp. Rev. Food Sc. Food Safety. 12, 652-661.

Nair, G.B., Ramamurthy, T., Bhattacharya, S.K., Dutta, B., Takeda, Y., Sack, D.A. 2007. Global dissemination of *Vibrio parahaemolyticus* serotype O3:K6 and its serovariants. Clin. Microbiol. Rev. 20, 39–48.

Nordstrom, J.L., Vickery, M.C.L., Blackstone, G.M., Murray, S.L., DePaola, A. 2007. Development of a multiplex real-time PCR assay with an internal amplification control for the detection of total and pathogenic *Vibrio parahaemolyticus* bacteria in oysters. Appl. Environ. Microbiol. 73, 5840-5847.

Oberbeckmann, S., Wichels, A., Wiltshire, K.H. Gerdts. 2011. Occurrence of *Vibrio parahaemolyticus* and *Vibrio alginolyticus* in the German Bight over a seasonal cycle. Antonie van Leeuwenhoek 100:291-307.

R Core Team (2017). R: A language and environment for statistical computing. R Foundation for Statistical Computing, Vienna, Austria. https://www.R-project.org/.

Rehnstam-Holm, A.S., Atnur, V., Godhe, A. 2014. Defining the niche of *Vibrio parahaemolyticus* during pre- and post-monsoon seasons in the coastal Arabian Sea. Microb. Ecol. 67:57-65.

Solorzano, L. 1969. Determination of ammonia in natural waters by phenol hypochlorite method. Limno. Oceanogr. 14 (1969), pp. 799–801

Strickland, J.D.H. and Parsons, T.R. 1968. Determination of reactive nitrite. In: *A Practical Handbook of Seawater Analysis*. Fish. Res. Board Canada Bull. 167, 71-75.

Urquhart, E.A., Jones, S.H., Yu, J.W., Schuster, B.M., Marcinkiewicz, A.L., Whistler, C.A., Cooper, V.S. 2016. Environmental conditions associated with elevated *Vibrio parahaemolyticus* concentrations in Great Bay Estuary, New Hampshire. PLOS.

U.S. Food and Drug Administration. 2010. Microbiological Methods and Bacteriological Analytical Manual. Appendix 2: most-probable number from serial dilutions. http://www.fda.gov/Food/FoodScienceResearch/LaboratoryMethods/ucm109656.htm

US FDA [United States Food and Drug Administration]. 2015. National Shellfish Sanitation Program (NSSP) Guide for the control of molluscan shellfish, 2015 revision. http://www.fda.gov/Food/GuidanceRegulation/FederalStateFoodPrograms/ucm2006754.htm

Vandersea M.W., Kibler S.R, Van Sant S.B, Tester P.A., Sullivan K., Eckert G., Cammarata C., Reece K., Scott G., Place A., Holderied K., Hondolero D., Litaker R.W. 2017. qPCR assays for *Alexandrium fundyense* and *A. ostenfeldii* (Dinophyceae) identified from Alaskan waters and a review of species-specific *Alexandrium* molecular assays. Phycologia. 56(3):303-320.

VA-DEQ (Virginia Department of Environmental Quality). 2014. Quality assurance project plan (QAPP) for James River Chlorophyll-a Study. Special Study # 14098, Richmond, VA.

(http://www.deq.virginia.gov/Portals/0/DEQ/Water/WaterQualityStandards/James%20River%20Chl%20A%20Study/SAP_Reports/QAPP_JR_CHLa_Study_with_signatures.pdf)

Vezzulli L, Grande C, Reid PC, Hélaouet P, Edwards M, Hofle MG, Brettar I, Colwell RR, Pruzzo C. 2016. Climate influence on Vibrio and associated human diseases during the past half-century in the coastal North Atlantic. PNAS 113:E5062–E5071

Zimmerman, A.M., DePaola, A., Bowers, J.C., Krantz, J.A., Nordstrom, J.L., Johnson, C.N., Grimes, D.J. 2007. Variability of total and pathogenic *Vibrio parahaemolyticus* densities in Northern Gulf of Mexico water and oysters. Appl. Environ. Microbiol. 73:7589-7596.

Table 1: Summary of the type of samples collected during this study.

Data collected during this study	Frequency
Total and pathogenic *Vp* in oyster (MPN/g)	Biweekly
Total and pathogenic *Vp* in sediment (MPN/g)	Biweekly
Total and pathogenic *Vp* in water (MPN/mL)	Biweekly
Phytoplankton species composition (taxa/mL)	Biweekly
Zooplankton species composition (taxa/m^3)	Biweekly
Chlorophyll a (µg/L)	Biweekly
Phaeopigment (µg/L)	Biweekly
Ammonium (NH4) (µM/L)	Biweekly
Dissolved inorganic nitrogen (DIN) (µM/L)	Biweekly
Dissolved organic nitrogen (DON) (µM/L)	Biweekly
Phosphate (PO4) (µM/L)	Biweekly
Total Dissolved Phosphate (TDP) (µM/L)	Biweekly
Total Suspended Solids (TSS) (mg/L)	Biweekly
Water Temperature (˚C)	15 mins interval
Salinity (psu)	15 mins interval
pH	15 mins interval
Turbidity (NTU)	15 mins interval
Chlorophyll a (µg/L)	15 mins interval
Optical Dissolved Oxygen (mg/L)	15 mins interval

Table 2: Characterization of the sediment collected at the beginning of the study at each site.

Site	Gravel % ± std dev.	Sand % ± std dev.	Silt % ± std dev.	Clay % ± std dev.
Perrin	0%	37.4 %± 28.8	40.7% ± 25.0	21.8% ± 16.2
York	0%	96.4% ± 0.9	1.2% ± 1.3	2.4% ± 0.4

Table 3: Summary of the environmental data values collected by YSI sensors and grab samples collected approximately every 2 weeks. Values shown were calculated using the data recorded at time of sampling.

Measured Parameter	**Site**	**Mean ± std dev.**	**Range**
Water temperature (˚C)	Perrin	27.19 ± 3.34	20.90-30.81
	York	24.45 ± 3.32	18.15-27.91
Salinity (psu)	Perrin	15.45 ± 1.58	13.08-17.91
	York	16.46 ± 1.91	13.85-19.37
Turbidity (NTU)	Perrin	6.88 ± 4.23	2-16
	York	10.13 ± 4.58	1-15
Adjusted Chlorophyll a (µg/L)	Perrin	8.38 ± 4.68	2-15
	York	8.63 ± 4.74	1-16
pH	Perrin	7.65 ± 0.26	7.26-8.03
	York	7.83 ± 0.32	7.34-8.21
Dissolved Oxygen (mg/L)	Perrin	5.91 ± 1.53	3.38-7.25
	York	6.14 ± 2.09	2.46-8.45
NH_4 (mg/L)	Perrin	5.56 ± 3.49	2-13.60
	York	3.27 ± 2.23	0.45-7.46
DIN (mg/L)	Perrin	6.48 ± 3.57	2.30-14.40
	York	5.05 ± 3.34	0.77-12.08
DON (mg/L)	Perrin	28.11 ± 6.64	13.80-38.80
	York	21.71 ± 4.40	8.70-32.60
PO_4 (mg/L)	Perrin	0.51 ± 0.26	0.20-1.03
	York	0.41 ± 0.29	0.18-1.19
Total Dissolved Phosphate (mg/L)	Perrin	0.73 ± 0.41	0.15-1.61
	York	0.47 ± 0.35	0.15-1.32
Total Suspended Solids (mg/L)	Perrin	25.15 ± 7.04	16.47-40.50
	York	24.46 ± 8.83	10.00-39.33
Chlorophyll a (µg/L)	Perrin	16.04 ± 7.98	8.94-35.96
	York	15.94 ± 4.28	9.10-25.39
Phaeopigments (µg/L)	Perrin	7.15 ± 1.89	4.61-11.20
	York	8.08 ± 3.05	4.51-14.65

Table 4: Spearman's rank correlation coefficient between levels of *Vp* in the different matrices (p values are indicated such as: * $p < 0.05$; ** $p < 0.01$; *** $p < 0.0001$).

Matrices	***Vp tlh***	***Vp tdh***	***Vp trh***
Sediment & Water	0.434	0.513*	0.500*
Sediment & Oyster	0.004	0.585*	0.398
Water & Oyster	0.520*	0.554*	0.690**

Table 5: Spearman's rank correlation coefficient between levels of total and pathogenic *Vp* within each matrix (p values are indicated such as: * $p < 0.05$; ** $p < 0.01$; *** $p < 0.001$).

	Oyster	**Sediment**	**Water**
Vp tlh & Vp tdh	0.022	0.819**	0.729**
Vp tlh & Vp trh	-0.237	0.293	0.328

Fig. 1: Satellite Image showing the location of the 2 study sites. Aerial Distance between the 2 sites was about 6 kms.

Fig. 2: Water quality data recorded by the YSI sensors deployed at each study site.

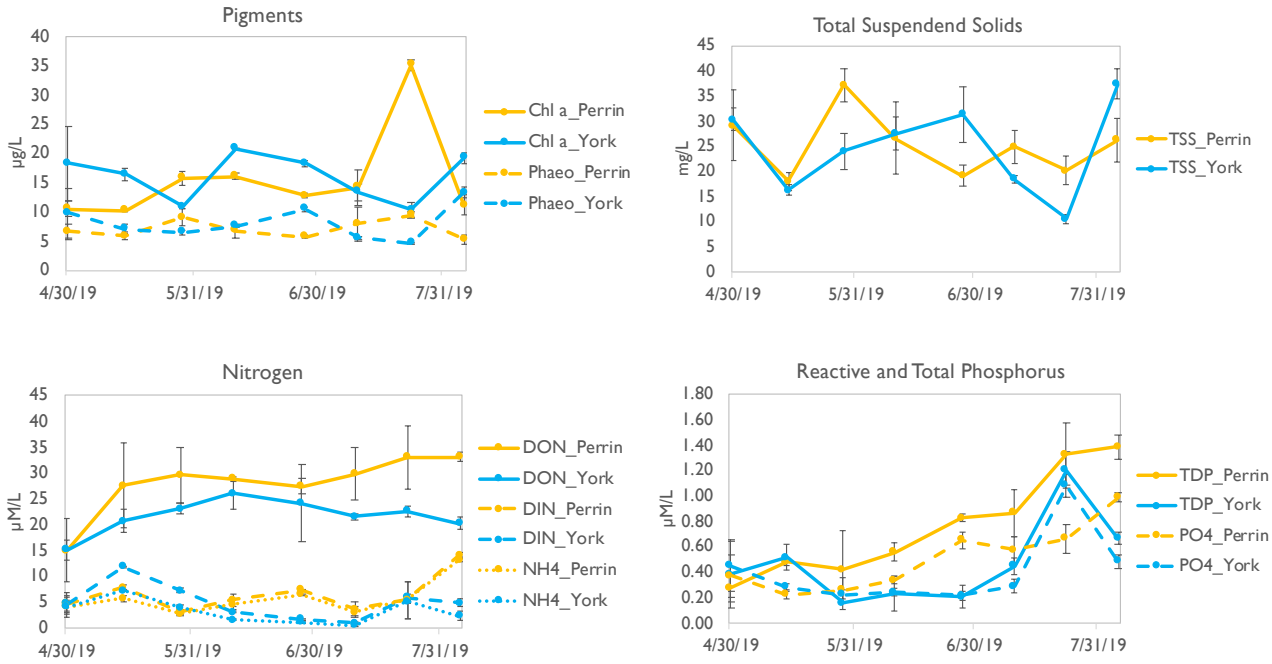

Fig. 3: Water quality parameters measured from grab samples collected at each sampling time point.

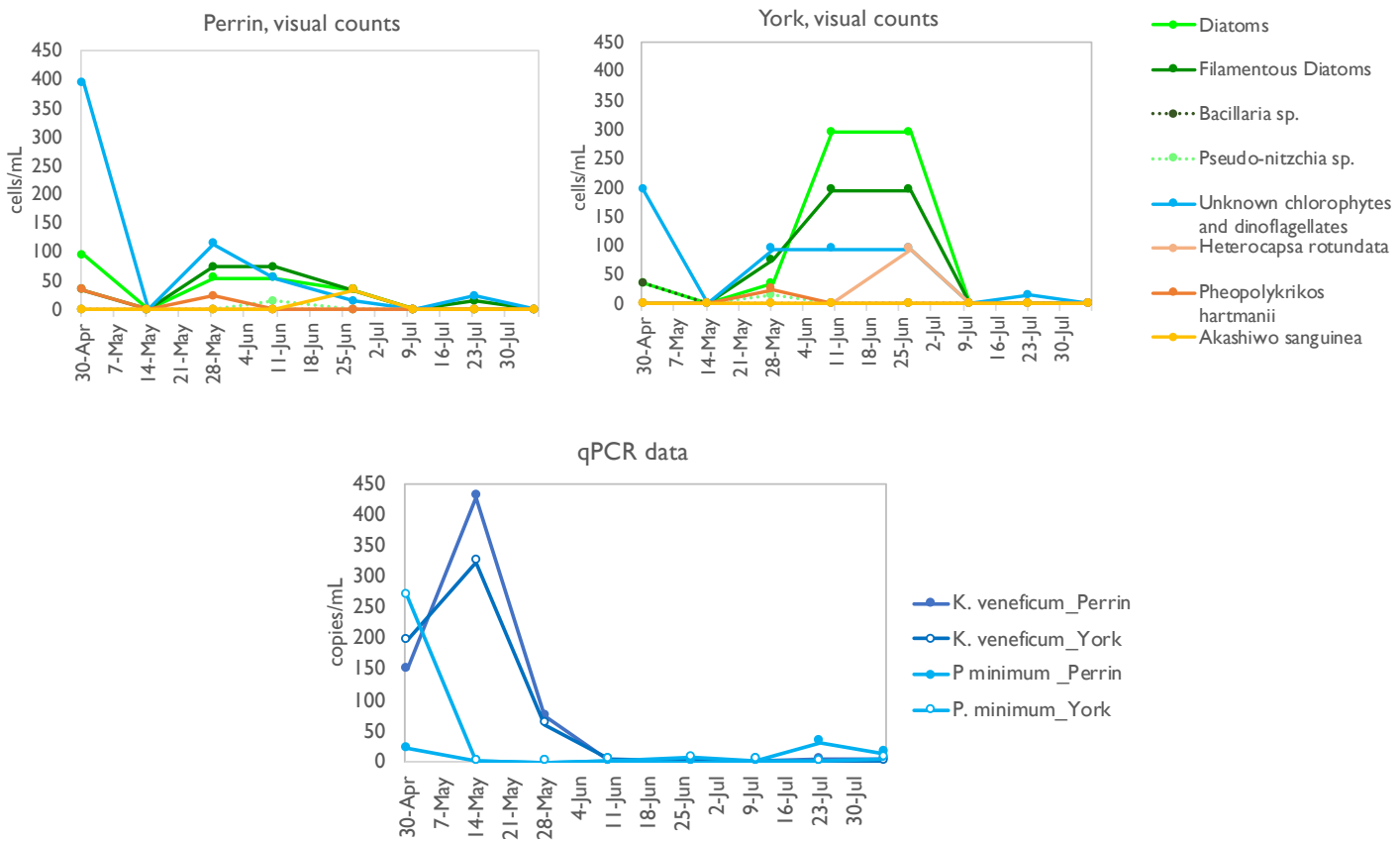

Fig. 4: Phytoplankton species composition results showing the data associated with visual counts (top graphs) and the data associated with qPCR (bottom graph).

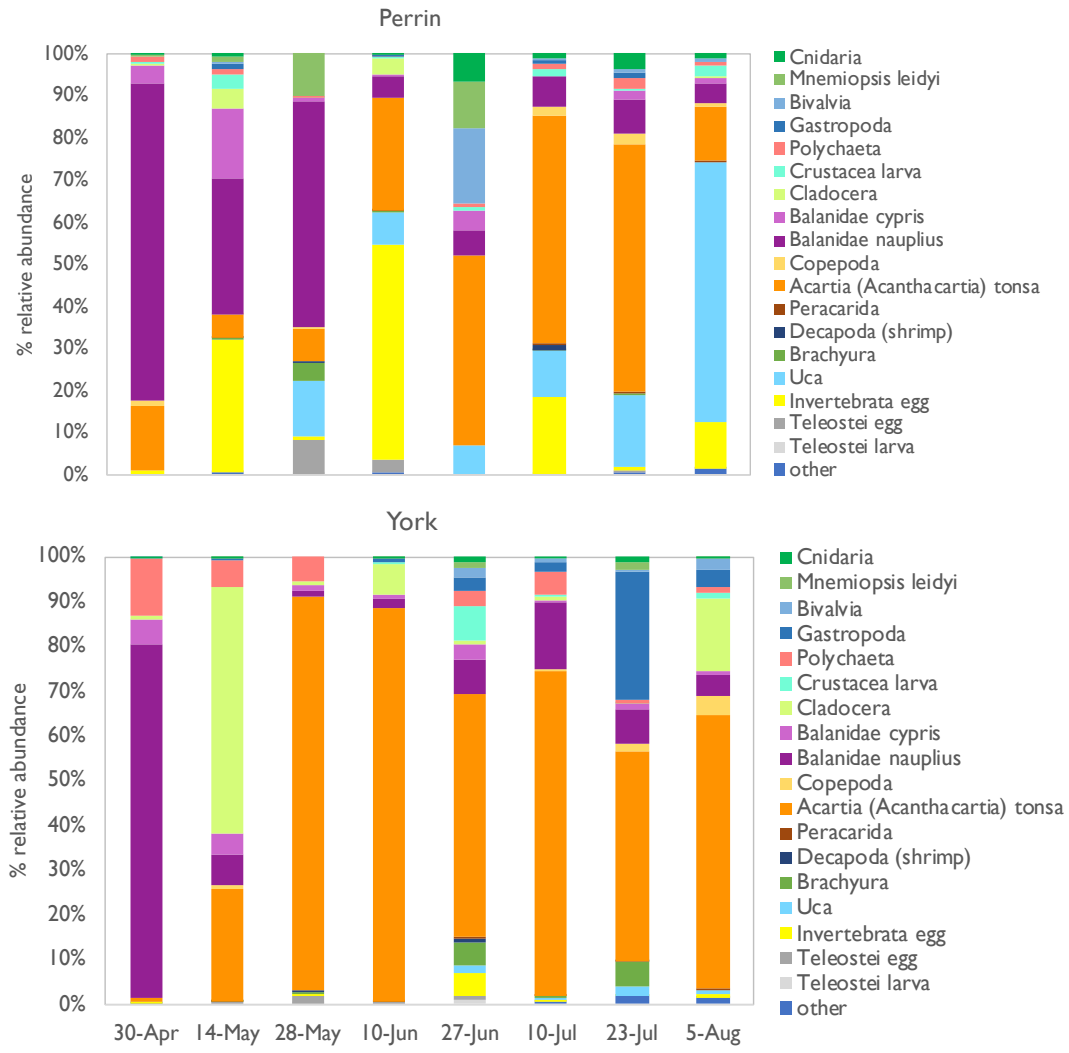

Fig. 5: Relative abundance of the zooplankton taxa identified in each sample.

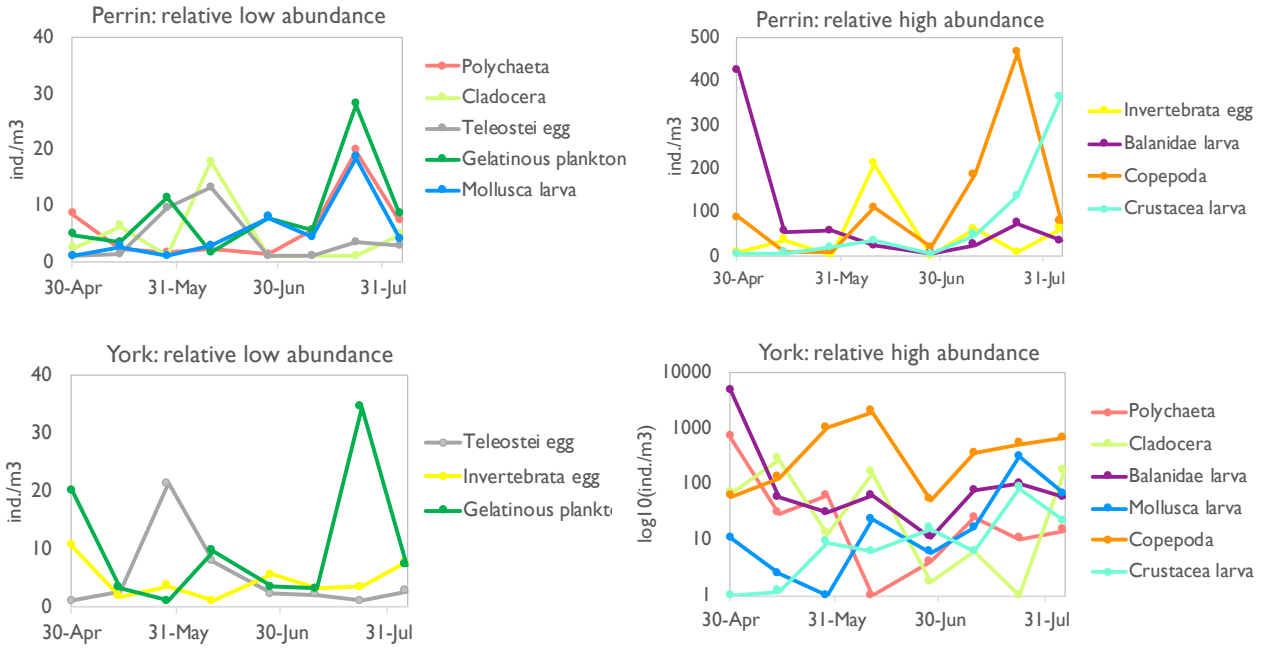

Fig. 6: Abundance of zooplankton taxa at each site. Plots on the left show taxa of relative low abundance, while plots on the right show taxa of relative high abundance. Due to the large number of taxa identified, taxa presented in this figure were in some instances grouped to allow for clearer graphical presentation of the data.

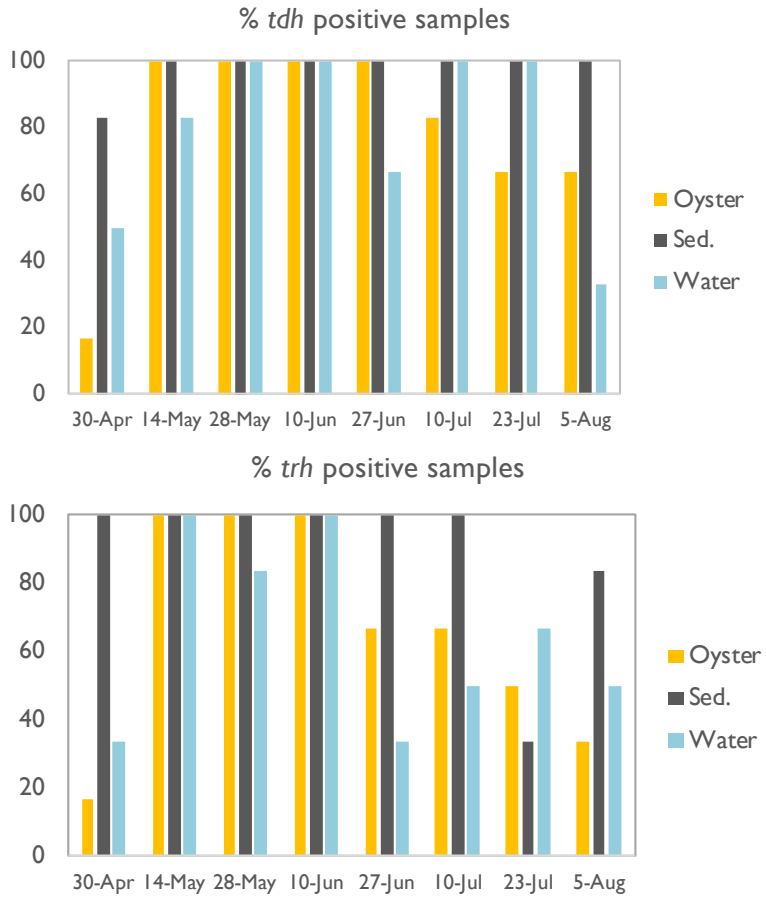

Fig. 7: Percentage of detection of *tdh* and *trh* genes in each matrice (data from each site were pooled).

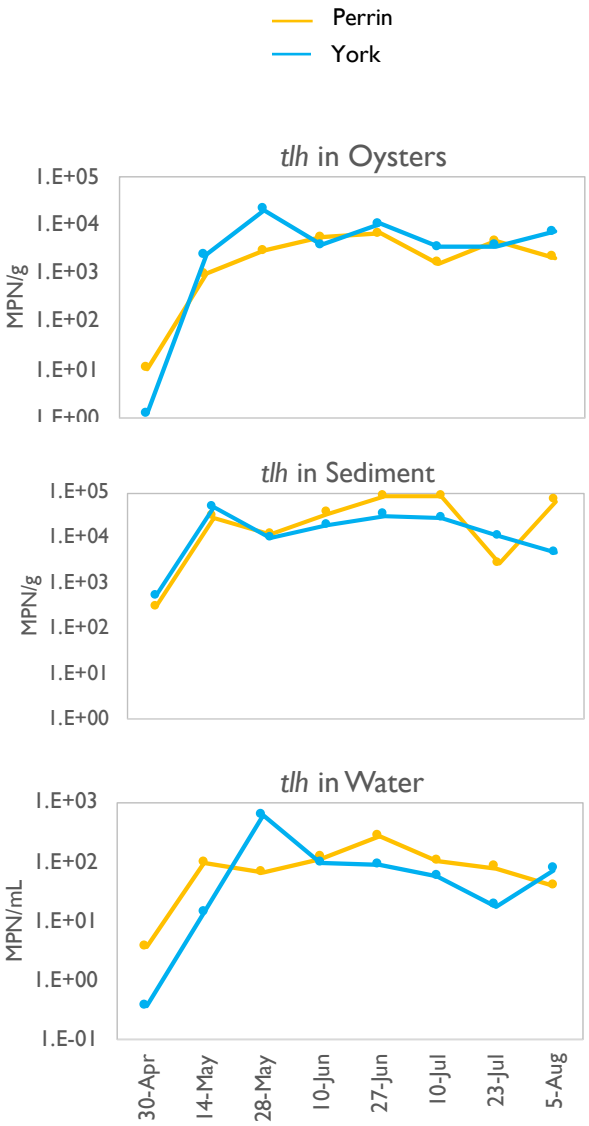

Fig. 8: Abundance in oyster, sediment and water samples of *Vp tlh* strains (total). Data presented are the geometric mean of 3 replicate samples per matrix.

Fig. 9 Abundance in oyster, sediment and water samples of *Vp* strains possessing the *tdh* (left panels) or the *trh* gene (right panels). Data presented are the geometric mean of 3 replicate samples per matrix.

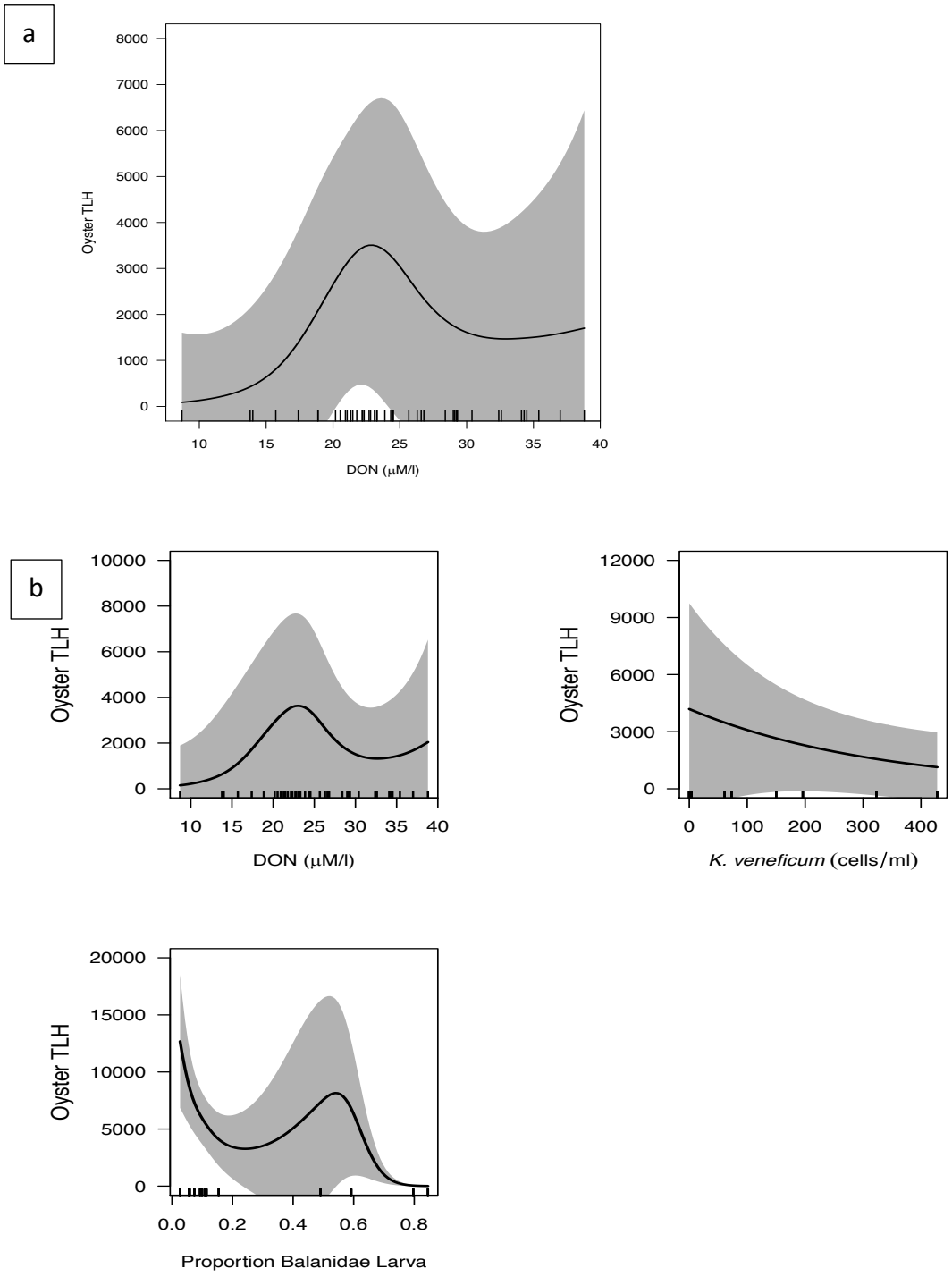

Fig. 10: Model predictions of mean *tlh* abundance in oyster over the observed domain of predictor variables that were retained: a/ model incorporating only DON; b/ model incorporating DON, *K. veneficum* abundance and Balanidae larvae. Rug on x-axes show observed values of predictors, and bootstrapped uncertainty (95% CI) is shown in grey shading.

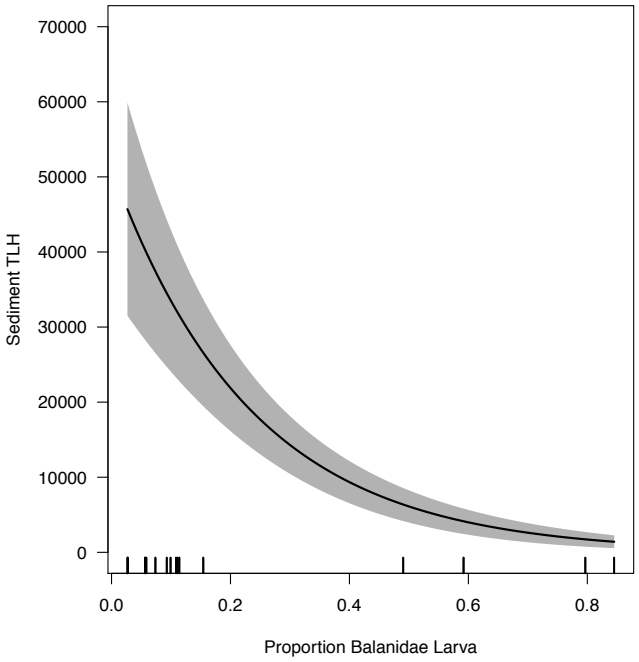

Fig. 11: Model predictions of mean *tlh* abundance in sediment over the observed domain of predictor variable(s) that was retained, i.e. Balanidae larvae. Rug on x-axes show observed values of predictors, and bootstrapped uncertainty (95% CI) is shown in grey shading.

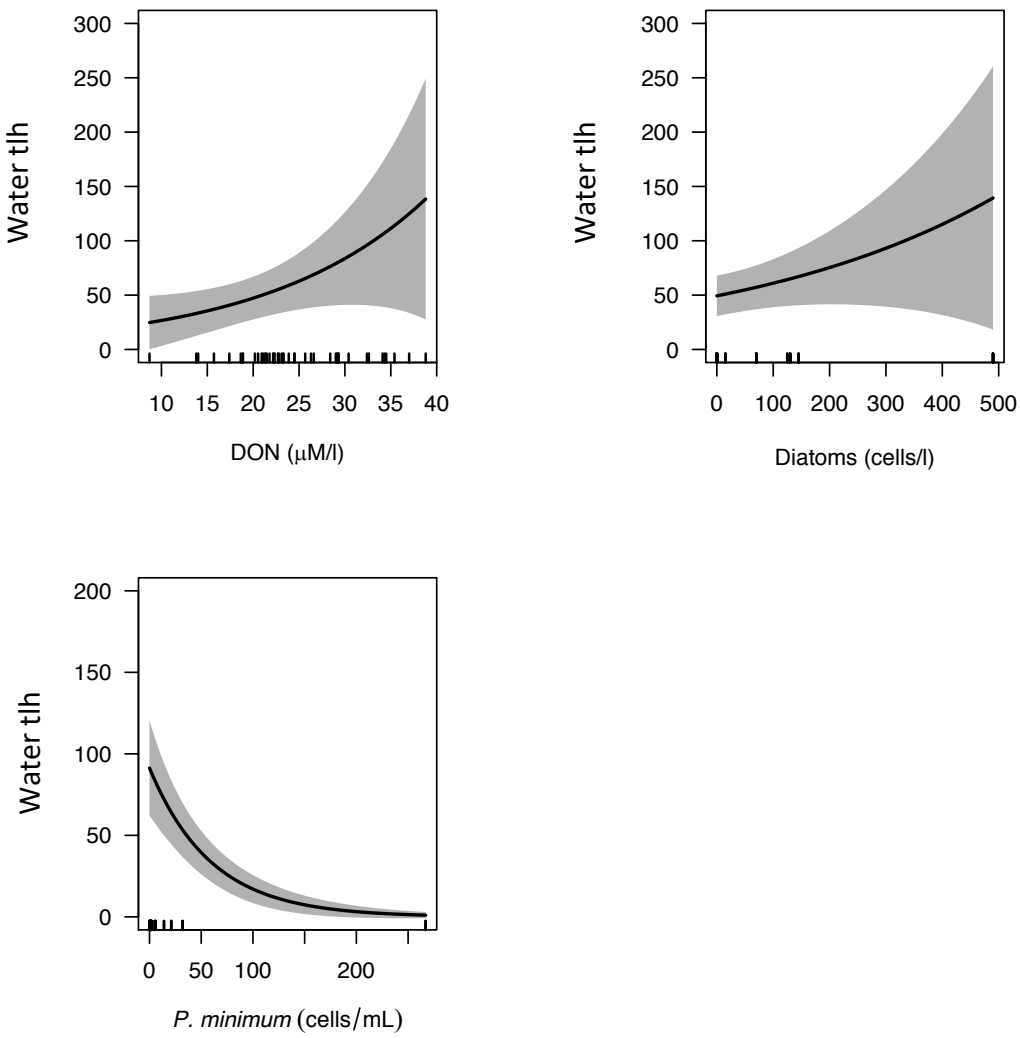

Fig. 12: Model predictions of mean *tlh* abundance in water over the observed domain of predictor variable(s) that was retained i.e. the model incorporating DON, Diatoms and *P. minimum*. Rug on x-axes show observed values of predictors, and bootstrapped uncertainty (95% CI) is shown in grey shading.

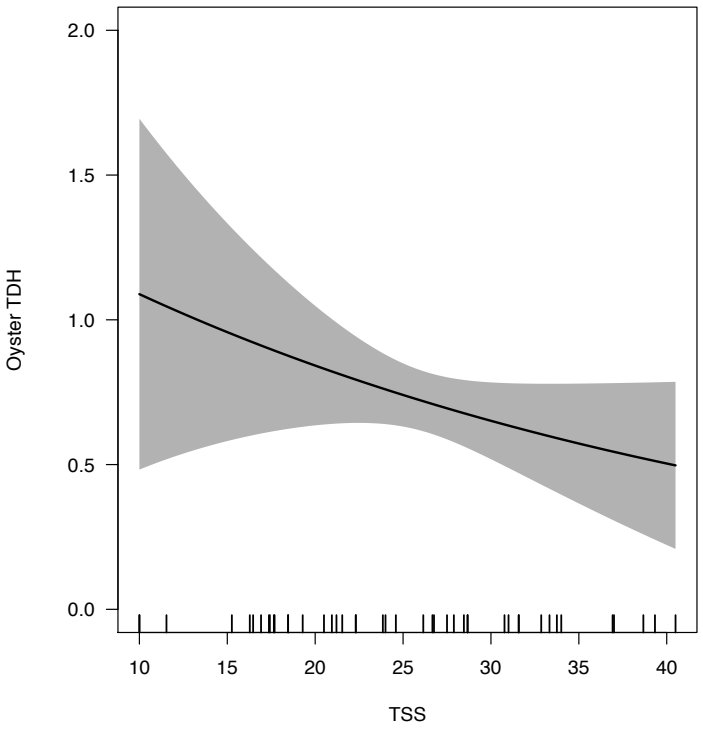

Fig. 13: Model predictions of mean *tdh* abundance in oyster over the observed domain of predictor variable(s) that was retained, i.e. TSS. Rug on x-axes show observed values of predictors, and bootstrapped uncertainty (95% CI) is shown in grey shading.

a

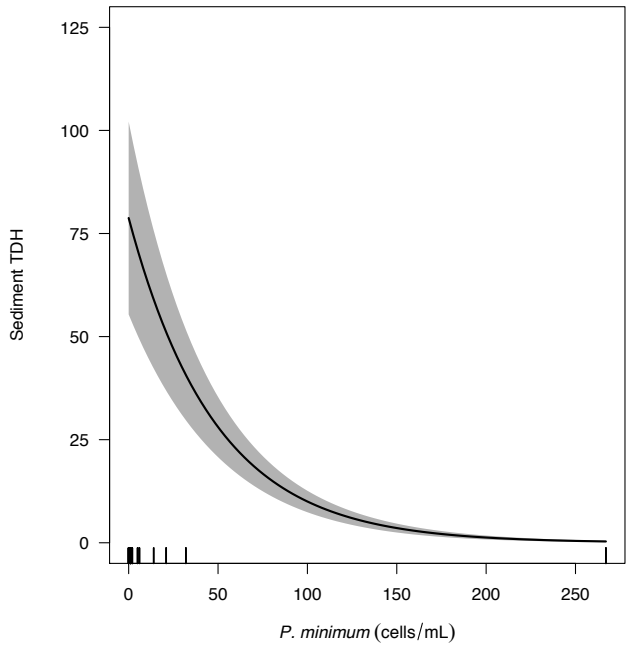

b

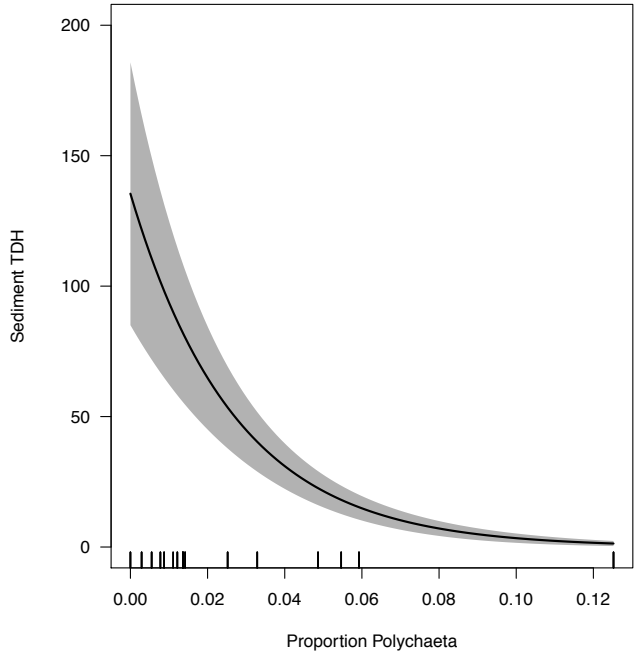

Fig. 14: Model predictions of mean *tdh* abundance in sediment over the observed domain of predictor variable(s) that were retained: a/ model incorporating *P. minimum* and b/ model incorporating Polychaeta larvae. Rug on x-axes show observed values of predictors, and bootstrapped uncertainty (95% CI) is shown in grey shading.

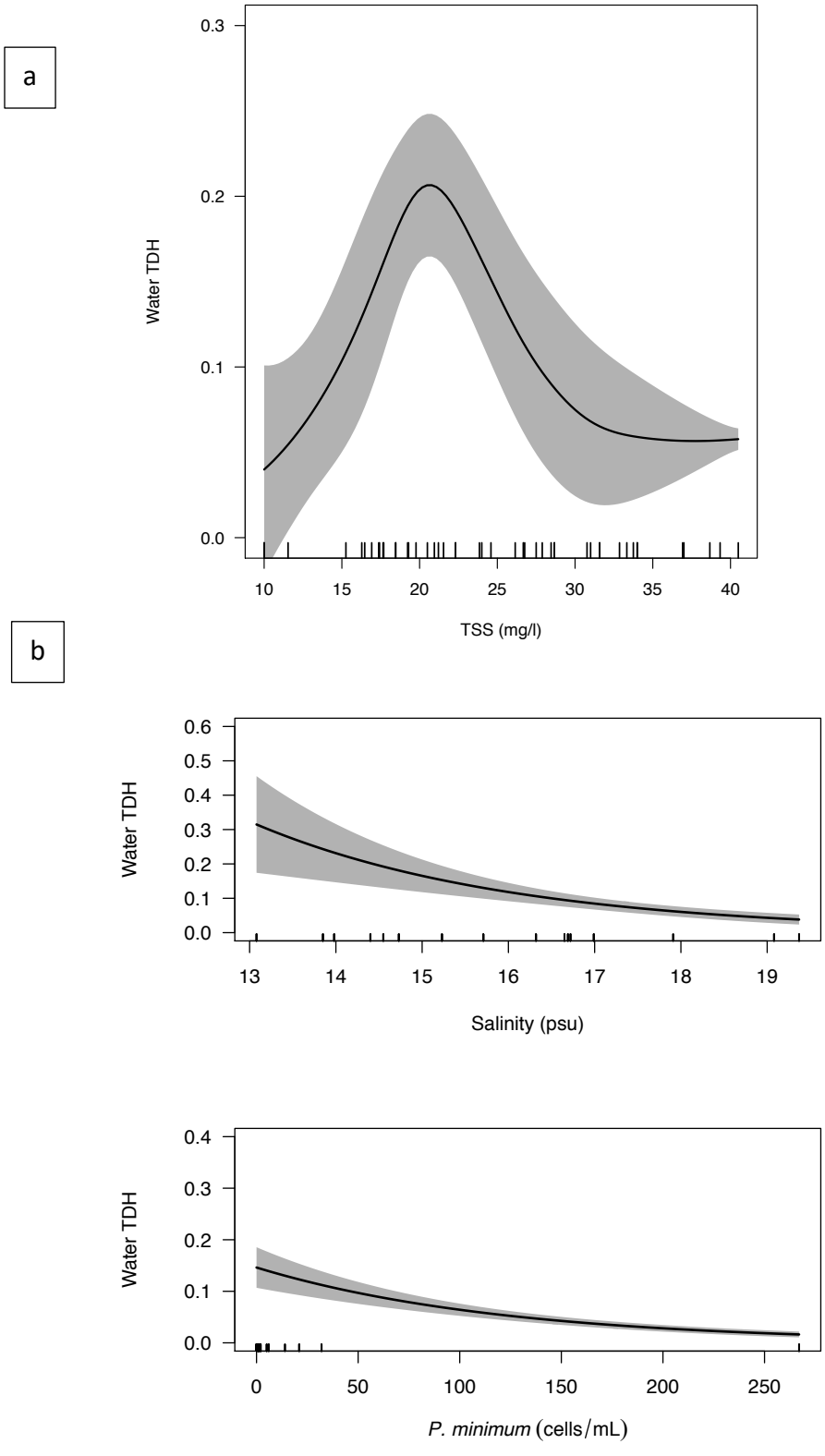

Fig. 15: Model predictions of mean *tdh* abundance in water over the observed domain of predictor variable(s) that were retained: a/ model incorporating TSS and b/ model incorporating salinity and *P. minimum*. Rug on x-axes show observed values of predictors, and bootstrapped uncertainty (95% CI) is shown in grey shading.

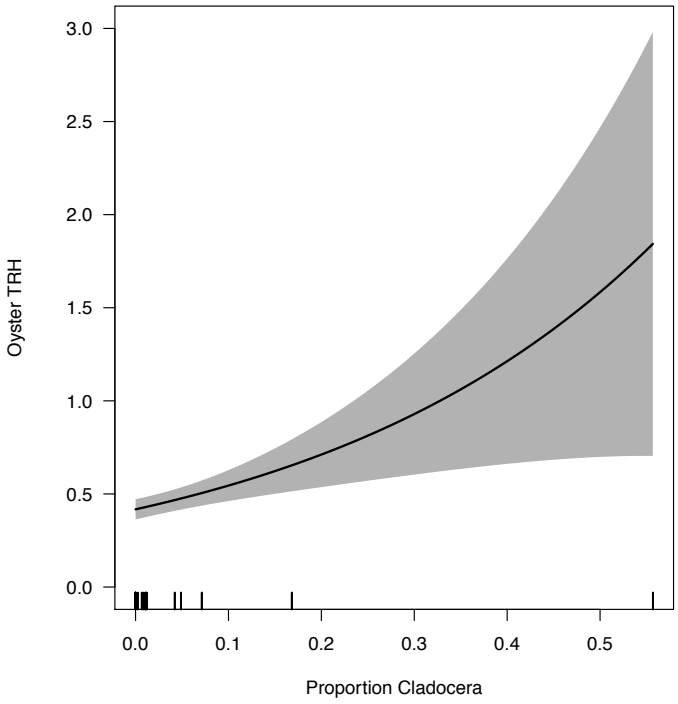

Fig. 16: Model predictions of mean *trh* abundance in oyster over the observed domain of predictor variable(s) that was retained, i.e. Cladocera. Rug on x-axes show observed values of predictors, and bootstrapped uncertainty (95% CI) is shown in grey shading.

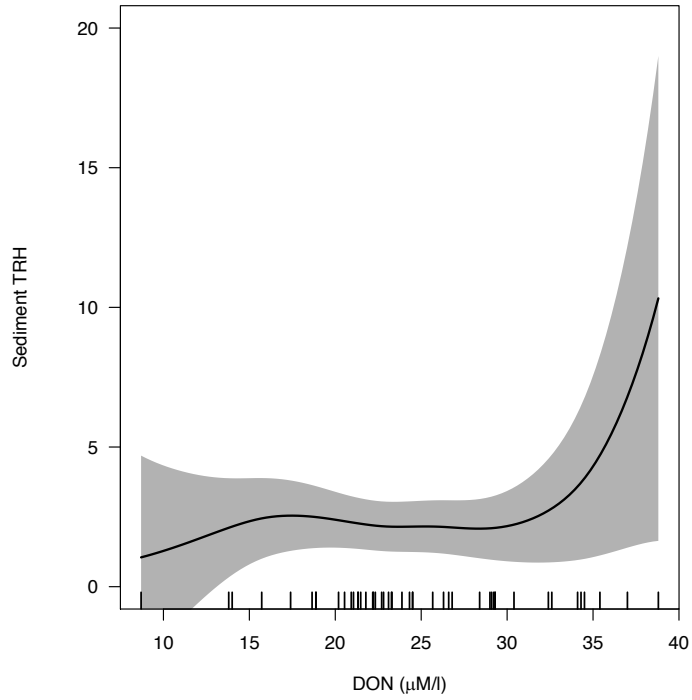

Fig. 17: Model predictions of mean *trh* abundance in sediment over the observed domain of predictor variable(s) that was retained, i.e. DON. Rug on x-axes show observed values of predictors, and bootstrapped uncertainty (95% CI) is shown in grey shading.

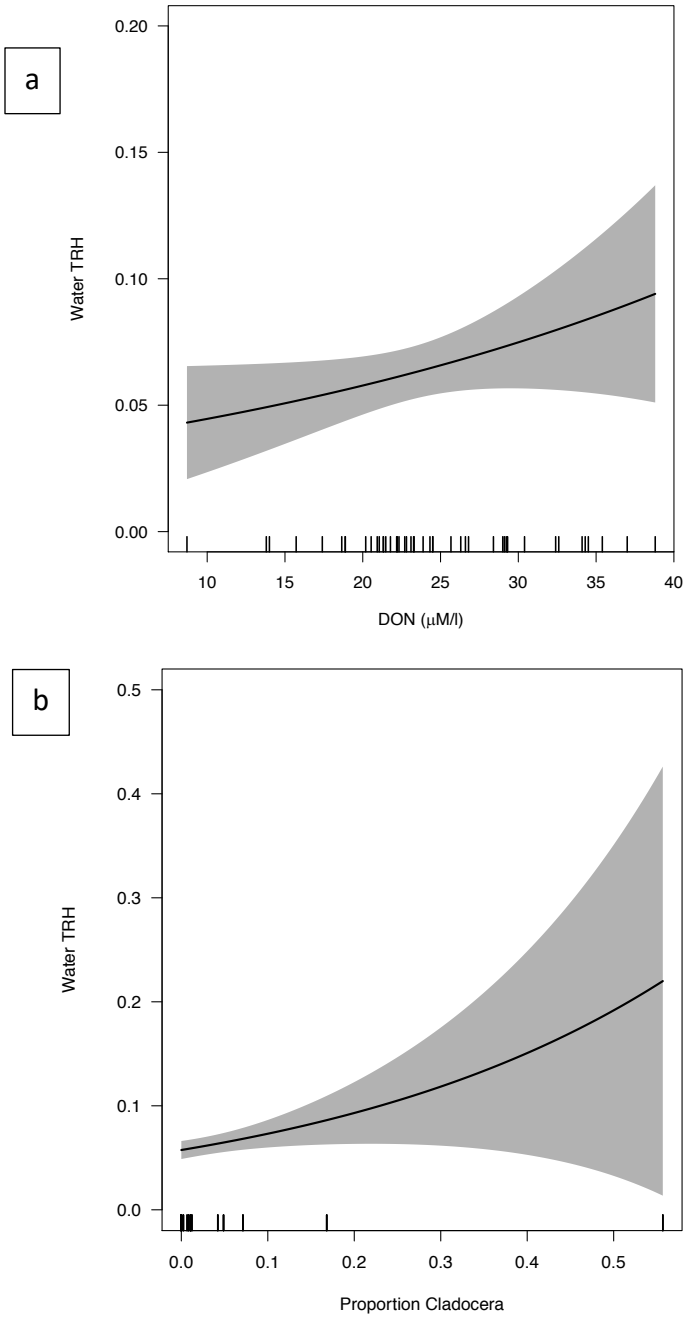

Fig. 18: Model predictions of mean *trh* abundance in water over the observed domain of predictor variable(s) that were retained: a/ model incorporating DON and b/ model incorporating Cladocera. Rug on x-axes show observed values of predictors, and bootstrapped uncertainty (95% CI) is shown in grey shading.